Nonlinear Mechanooptical Behavior of Poly(ethylene naphthalate)/ Poly(ether imide) Blends. Dynamic Phase Behavior

K. Kanuga and M. Cakmak*

Polymer Engineering Institute, University of Akron, Akron, Ohio 44325-0301

Received June 3, 2005; Revised Manuscript Received September 19, 2005

ABSTRACT: The mechanooptical behavior and structural organization processes in melt miscible PEN−PEI blends have been investigated in the rubbery state as influenced by blend composition, stretching temperature, and deformation rate. This was accomplished using a spectral birefringence system integrated in a specially built uniaxial stretching machine[1,2] where real-time birefringence, true stress, and true strain are monitored during the course of the deformation. Three distinct stress−optical regimes have been observed with an additional glassy component. The final structure and deformation behavior of the blends have been mapped out in a dynamic phase diagram showing that the material undergoes three critical structural transitions. At low temperatures near T_g the polymer remains in a nematic-like state, and orientation-induced crystallization occurs only above a certain stretching temperature. At intermediate temperatures the liquid−liquid (T_{ll}) transition occurs wherein the material transforms from a "structured liquid" to a "true liquid" state at ($1.08T_g$ (K)) exhibited by the disappearance of the initial glassy component as the material becomes devoid of the segmental correlations. At higher temperatures, where the relaxation process dominates and where the thermal induced crystallization is still suppressed, the material was found to remain in the amorphous state even after being stretched to large deformation levels.

I. Introduction

PEN (poly(ethylene naphthalate)) is a slow crystallizing polymer with a moderately high glass transition temperature of around 120 °C. The chemical structure of PEN is similar to PET with the exception of the naphthalene rings, which makes PEN chains stiffer than PET. This polymer, like PET, can be quenched into an amorphous state, and it can also be crystallized either by slow cooling from the melt or by stretching between the glass transition temperature and the cold crystallization temperature.[3] One of the unusual characteristics of PEN is that it shows necking upon stretching from the amorphous state above the glass transition temperature which is caused due to the highly cooperative orientation of naphthalene planes parallel to the surface of the film.[3] Blending of poly(ether imide) (PEI) with PEN has been shown to eradicate necking by hindering the alignment of the naphthalene rings[4] which makes the PEN−PEI blend an attractive material due to its high glass transition temperature and good barrier properties coupled with better processability. PEN and its blends hence have the potential to be used extensively for bottles and high-performance film applications that require deformation of the polymer above its glass transition temperature, causing significant polymer orientation, crystallization, and a sequence of structural ordering processes which ultimately determine the physical properties of the product. Moreover, polymer orientation and crystallization processes are controlled by the stretching temperature and deformation rate. Hence, it is critical to study the effect of temperature and deformation rate as well as the structural organization processes taking place during deformation to control the properties of the final product.

* Corresponding author: e-mail cakmak@uakron.edu, Ph 330 972 6928.

There have been numerous studies[5−10] on the effect that deformation has on the structure by off-line techniques. These "after the fact" studies did not lend themselves in unraveling the complex sequence of structural events as later processes tend to mask the earlier ones. Recently, synchrotron X-ray studies have been performed on PET while the samples were being uniaxially stretched.[11] These studies provided insight into the fast structural organization process occurring during stretching, particularly after the crystalline phase is formed. Birefringence as an overall measure of the optical anisotropy of materials is a robust technique that gives detailed quantitative insight into the mechanistic changes in the structural organization and ordering processes particularly when it is captured in real time along with true mechanical behavior.[12,13] Studies on the structural details using birefringence have been reported wherein the birefringence−stress behavior during deformation in the rubbery state has been investigated in PET,[14] PEN,[7,15] and some amorphous polymers such as PS and PC.[16] However, detailed and quantitative studies on the associated structural ordering mechanisms during stretching along with the effect of stretching rate and temperature on highly deformed polymer systems have not been performed, all of which can have a significant effect on the final properties of the product. Moreover, there is no single literature which deals with the stress−optical behavior and the associated structural details in polymer blends.

In this regard, an investigation was conducted on the mechanooptical behavior of PEN−PEI blend films in the rubbery state as influenced by blend composition, stretching temperature, and deformation rate. Using the newly developed stretching system,[1,2] we acquired birefringence simultaneously with true mechanical behavior of the material at every 0.2 s as it is being subjected to large deformations. These studies coupled

10.1021/ma0511595 CCC: $30.25
Published on Web 10/20/2005

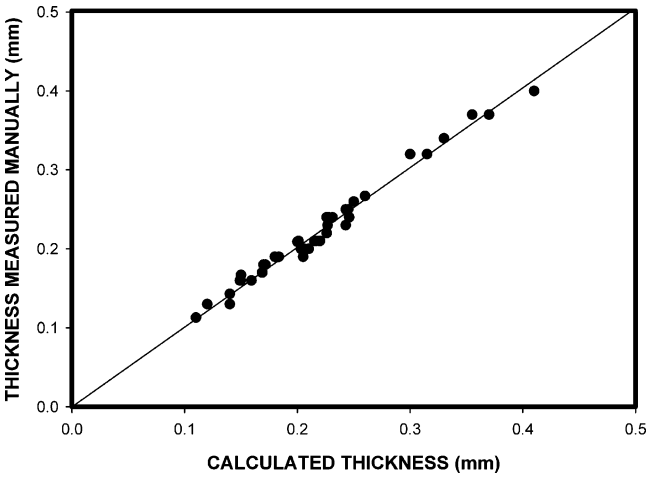

Figure 1. On-line (using incompressibility assumption) vs off-line thickness measurements (using precision micrometer).

with other standard off-line techniques were used to assess the linear and nonlinear mechanooptical behavior as well as the structural organizational processes taking place during stretching and eventually map out in detail the final structure and deformation behavior of the material as a function of blend composition, stretching temperature, and rate.

II. Experimental Procedures

Materials. Poly(ethylene 2,6 naphthalene dicarboxylate) (PEN) with an intrinsic viscosity of 0.86 dL/g was used in this study and was provided in pellet form by Eastman Co. Poly(ether imide) (PEI) with an intrinsic viscosity of 0.61 dL/g was supplied by the General Electric Co. in pellet form (Ultem 1000). A series of PEN/PEI blends ranging from 100/0 to 80/20 in composition were prepared using a Werner and Pfleiderer corotating twin-screw extruder (ZSK-30). The melt temperature at the die was set at 305 °C, and the extrudates were subsequently quenched in the water bath and pelletized. The film preparation procedure can be found elsewhere.[4]

On-Line Birefringence and True Mechanical Behavior Measurements. A uniaxial stretching machine developed in our group[1,2] was used to simultaneously determine the mechanical and optical properties of PEN films during deformation. The machine is essentially composed of three parts: the uniaxial stretching machine with environmental chamber, the spectral birefringence system, and a laser micrometer system that continuously measures the width of films during stretching. Real-time measurements of optical retardation, sample width, force, and elongation are recorded simultaneously. Assuming (1) simple extension and (2) incompressibility, the time variation of the local thickness is calculated, and thus birefringence, local true stress, and local true strain are determined.

A change in volume due to the development of crystallinity in the material would be expected to occur. But as will be shown in this paper, the degree of crystallinity developed in the samples ranges anywhere from 0% to 30%. The volume change between these states is ~2.5% (ρ_c = 1.407 g/cm^3,[17] ρ_a = 1.325 g/cm^3 [18]).

Since the development of crystallinity is concentrated toward the end of stretching, the error committed by the incompressibility assumption is negligible. In addition, assuming any change in volume would affect all dimensions equally and the width being measured in real time reduces the committed error. We have verified this assumption with off-line thickness measurements taken for different stretch ratios as well as different stretching conditions and compared them with on-line thickness values obtained from width measurements. These data are shown in Figure 1 where good correlation is observed between them. Additional details of the system can be found elsewhere.[1,2] The birefringence measurements taken in this study are reported for the wavelength of 546 nm.

Sample Preparation. Dumbbell-shaped specimens were cut from the original melt-cast and amorphous films and had the following dimensions: 75 mm long, 40 mm wide, and 30 mm wide in the narrowest region as shown below in the diagram. The samples were clamped and fixed in the arms of the uniaxial stretching system inside the environmental oven. In this real-time measurement system the laser micrometer continuously monitors sample width at the narrowest portion of the sample.

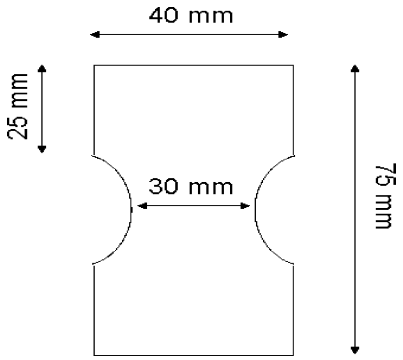

Thermal Characterization. The thermal properties of PEN and its blends with PEI were measured using a universal 2920 MDSC V2.6A TA Instruments DSC. The samples of ~6−10 mg were scanned at a heating rate of 20 °C/min under a dry nitrogen blanket. The reported transition temperatures (T_{cc}, T_m) refer to the peak maximum position. The degree of crystallinity of the blends was determined using the following equation and was normalized to the fraction of PEN present in the blends:

$$\text{crystallinity (\%)} = (\Delta H_{exp}/\Delta H^\circ) \times 100$$

where $\Delta H_{exp} = \Delta H_{melting} - \Delta H_{cold\ crystallization}$ and ΔH° is the heat of fusion for 100% crystalline PEN, which is 103.4 J/g.[19]

WAXD Measurements. A Bruker AXS generator equipped with a copper target tube and a two-dimensional detector was used to obtain the one-quadrant WAXD patterns of uniaxially oriented samples. The generator was operated at 40 kV and 40 mA with a beam monochromatized to Cu Kα radiation. A typical exposure time of 20 min was used.

The crystal size was measured using the Scherrer equation wherein the Bruker X-ray machine is used to collect intensity data as a function of scattering angle (2θ). The data collected are then used to calculate half-width of the (010) peak as well as the maximum scattering angle. The equation is given as

$$L_{hkl} = \frac{K\lambda}{\beta_0 \cos\theta}$$

where L_{hkl} is the mean dimension of the crystallites perpendicular to the planes (hkl), β_0 is the integral breadth or breadth at half-maximum intensity of the pure reflection profile in unit of radians, and K is a constant that is commonly assigned a value of unity.

The crystalline orientation factor was determined by taking the azimuthal scan through the diffraction angle corresponding to the plane of interest. Curve-fitting software was used to remove the intensity contribution from the off-equatorial peaks, finally obtaining the pure equatorial intensity profiles for the required plane. The intensity contribution from the background amorphous material was then subtracted from the intensity profiles to obtain the intensity of the pure crystalline

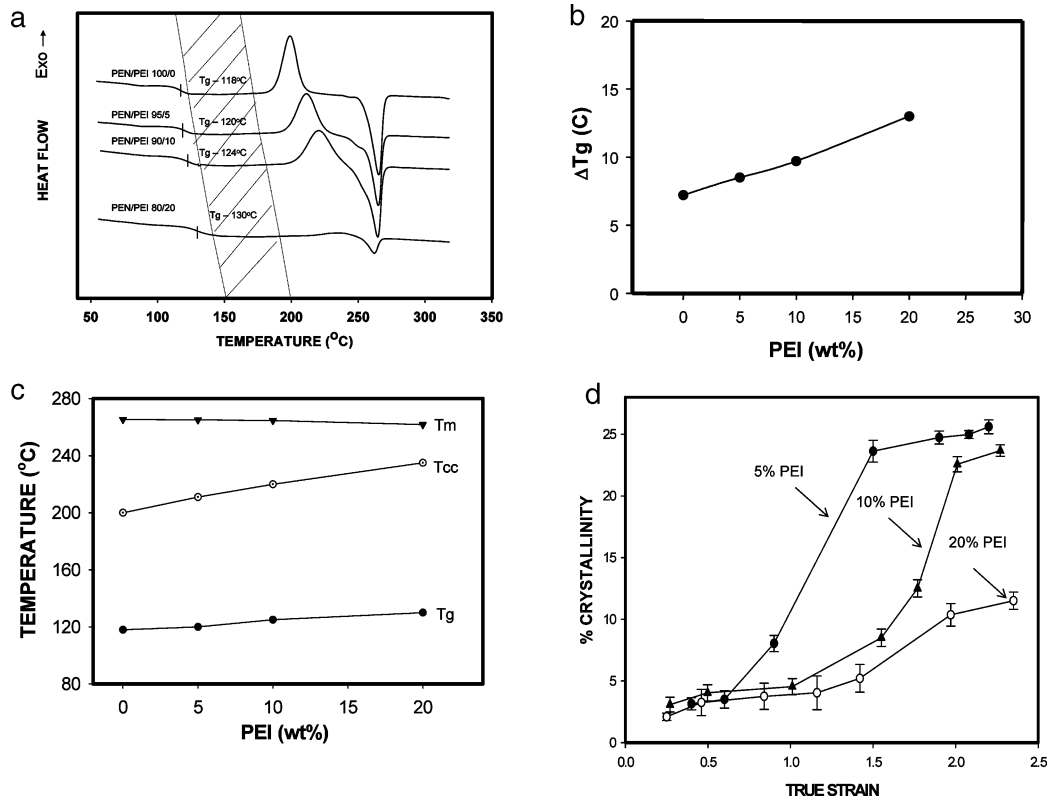

Figure 2. (a) DSC thermograms of melt-cast films. Dotted area marks the stretching window. (b) T_g breadth as a function of blend composition. (c) Change in T_g, T_{cc}, and T_m as a function of blend composition. (d) Change in % crystallinity as a function of stretch ratio.

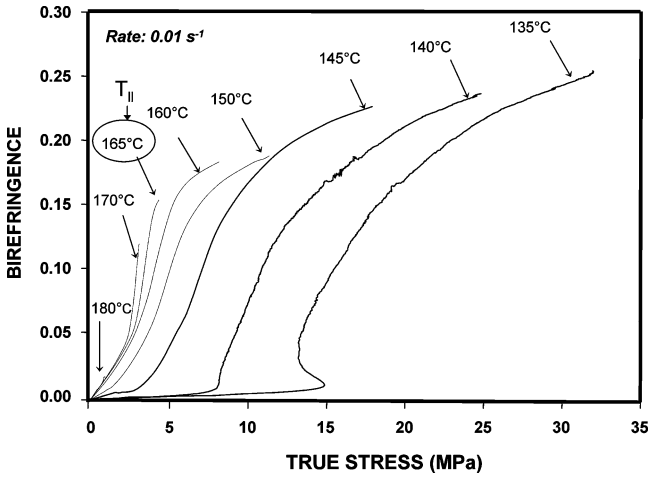

Figure 3. Temperature effect on the stress−optical behavior of the 20% PEI blend stretched at engineering strain rate of 0.01 s^{-1} and final stretch ratio 4×.

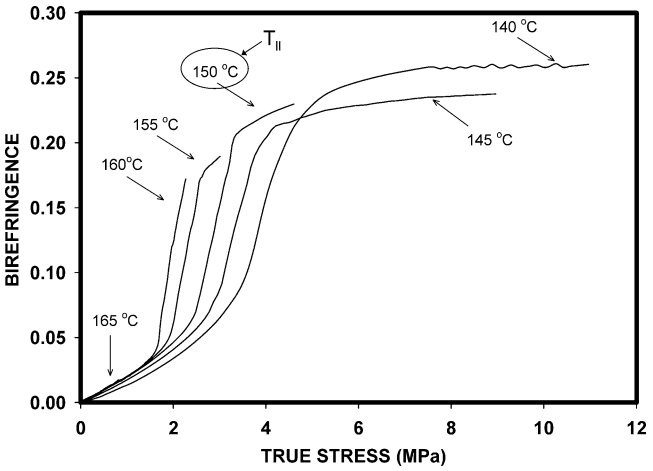

Figure 4. Temperature effect on the stress−optical behavior of the 5% PEI blend stretched at engineering strain rate of 0.01 s^{-1} and final stretch ratio 4×.

material. The $\cos^2\chi$ values were determined from the following equation.

$$\cos^2\chi(hkl,z) = \frac{\int_0^{\pi/2} I(\chi_{\text{corrected}}) \sin\chi \cos^2\chi \, d\chi}{\int_0^{\pi/2} I(\chi_{\text{corrected}}) \sin\chi \, d\chi}$$

To determine the orientation factor for the chain axis, we have defined a pseudo-orthorhombic unit cell for the PEN single chain. The details regarding the axis of the new unit cell as well as the angles between the axis of the pseudo-orthorhombic cell and the poles of the selected planes of the original triclinic unit cell are given in an earlier paper.[3]

From Wilchinsky's rule the $\cos^2\chi$ values of the chain (*C*-axis) become

$$\cos^2\chi(c,z) = \frac{(e_2^2 - f_2^2)\cos^2\chi(100,z) - (e_1^2 - f_1^2)(\cos^2\chi(100,z) + e_1^2 f_2^2 - e_2^2 f_1^2}{e_1^2 f_2^2 - e_2^2 f_1^2}$$

Here e, f, and g are the direction cosines for each plane. Finally, the orientation factor is given by

$$f_c = \frac{(3\langle\cos^2\chi_{c,z}\rangle - 1)}{2}$$

FT-IR Measurements. FTIR spectroscopy was performed using Digilab Excalibur series FT-IR to determine the preferential orientation of the amorphous phase of PEN and PEI chains independently. Since the thickness of the films exceeded 100 μm, an ATR technique using KRS-5 crystal (incident angle

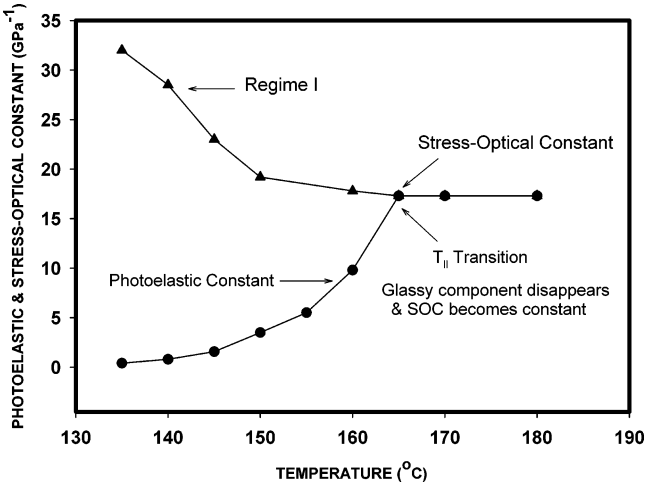

Figure 5. Photoelastic and regime I slope as a function of temperature for the 20% PEI blend stretched at engineering strain rate of 0.01 s^{-1} and final stretch ratio 4×.

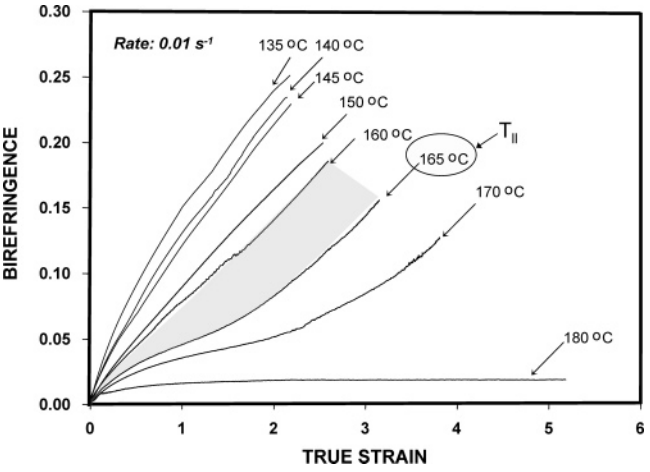

Figure 6. Temperature effect on the strain−optical behavior of the 20% PEI blend stretched at engineering strain rate of 0.01 s^{-1} and final stretch ratio 4×.

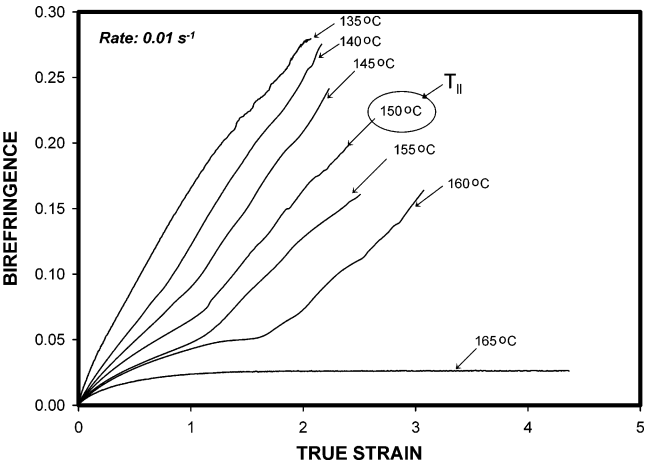

Figure 7. Temperature effect on the strain−optical behavior of the 5% PEI blend stretched at engineering strain rate of 0.01 s^{-1} and final stretch ratio 4×.

45°) and a ZnSe polarizer was adopted. The 64 scans with a resolution of 4 cm^{-1} were averaged to obtain a good signal-to-noise ratio. Two specific bands each corresponding to PEN and PEI individually were identified. The band at 1338 cm^{-1} was used to measure the orientation of PEN which corresponds to the CH_2 linkages, while the 1356 cm^{-1} band was used for PEI which corresponds to the imide linkage. Four components of

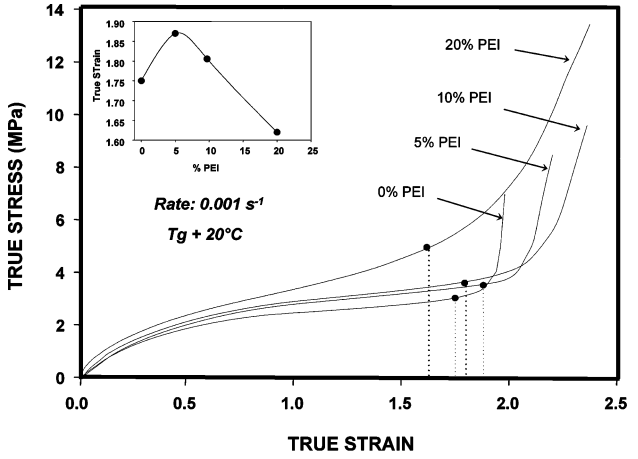

Figure 8. Effect of blend composition on the true stress−true strain curve at engineering strain rate of 0.001 s^{-1} and stretch ratio 4×.

the polarized ATR spectrum, namely $A_{TE,x}$, $A_{TM,x}$, $A_{TE,y}$, and $A_{TM,y}$, were obtained by rotating the sample as well as the polarizer by 90°, where TE indicates transverse electric polarization parallel to the film plane, TM indicates transverse magnetic polarization perpendicular to the film plane, the x axis denotes the draw direction, and y is the transverse direction. For instance, the notation $A_{TE,x}$ means that the draw direction of the sample is parallel to the plane of incidence, and the electric vector lies in the plane of incidence. The TE or TM geometries are obtained through changes in polarization of the incident beam by rotation of the polarizer, and so all four configurations can be attained by sample rotation on the ATR setup. The dichroic ratio (D_{xy}) was obtained from the above measurements using the procedure described elsewhere.[20] The orientation function was calculated from the dichroic ratio (D_{xy}) as defined by

$$f_{xy} = \left(\frac{D_{xy} - 1}{D_{xy} + 2}\right)\left(\frac{D_0 + 2}{D_0 - 1}\right)$$

where $D_0 = \cot^2 \alpha$, with α being the angle between the transition moment vector for the considered vibrational mode and the chain axis. The angle α for the bands selected is not accurately known, and hence an approximation of 0° is chosen since both 1338 and 1356 cm^{-1} are parallel bands.

III. Results and Discussion

Thermal Properties of As-Cast Films. As-prepared melt-cast samples are essentially amorphous, as shown in DSC thermograms for 100/0 PEN/PEI, 95/5 PEN/PEI, 90/10 PEN/PEI, and 80/20 PEN/PEI blends (Figure 2). The entire range of blends prepared exhibit a single T_g that shifts from 118 °C for plain PEN to 130 °C for 80/20 PEN/PEI blends, indicating good miscibility in the blend system. However, the T_g broadens with an increase in the PEI content (Figure 2a), suggesting that some microinhomogeneities are generated in the blend at higher PEI content. Crystallization from the amorphous state during heating is delayed with increasing PEI content as the mobility of PEN chains is suppressed with the addition of PEI; consequently, the cold crystallization temperature (T_{cc}) moves from 200 °C for 100/0 PEN/PEI to 235 °C for 80/20 PEN/PEI blend (Figure 2b). Moreover, the area under the crystallization peak also becomes smaller with the addition of PEI due to the dilution effect of amorphous PEI with the 20% PEI blend, causing the blend to significantly lose its ability to crystallize. Interestingly, the increase of T_{cc} is larger than the increase in T_g with increasing PEI concentra-

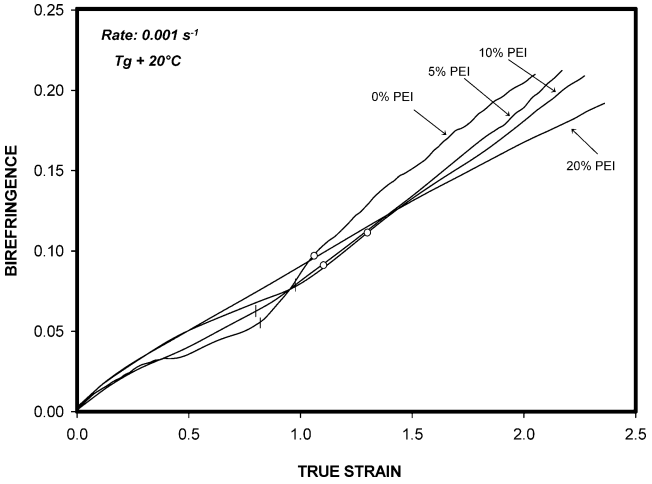

Figure 9. Effect of blend composition on the strain−optical behavior stretched at engineering strain rate of 0.001 s^{-1} and final stretch ratio 4×.

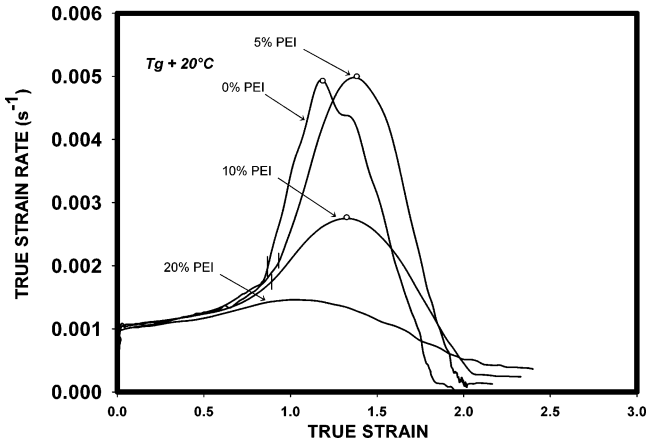

Figure 10. Effect of blend composition on the true strain rate behavior stretched at engineering strain rate of 0.001 s^{-1} macroscopic engineering strain rate.

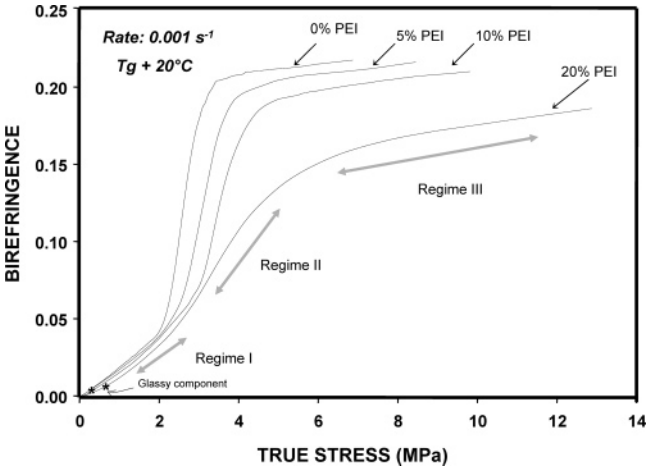

Figure 11. Effect of blend composition on the stress−optical behavior at engineering strain rate of 0.001 s^{-1} and stretch ratio 4×.

tion, leading to a widening of the T_g-T_{cc} window over which optimum stretching can be accomplished without the complications of thermal crystallization during stretching which may lead to optical haze and premature stoppage of deformation. The melting temperature T_m decreases with increasing PEI content following the normal melting point depression (Figure 2b).

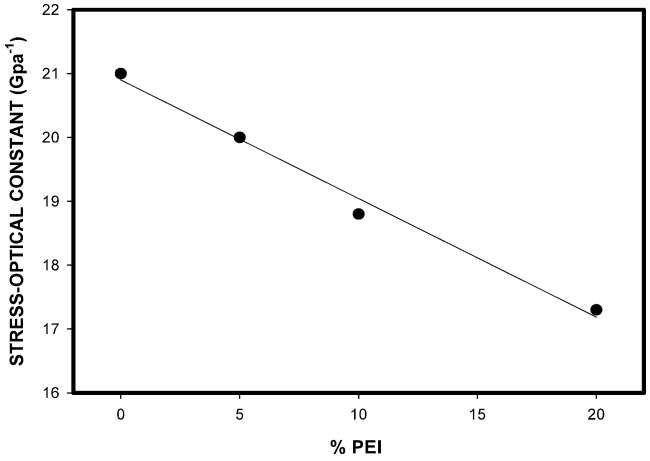

Figure 12. Stress−optical constant (SOC) as a function of blend composition.

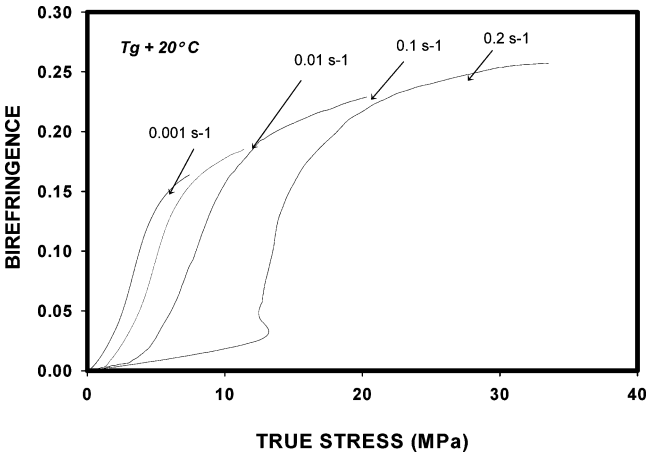

Figure 13. Rate effect on the strain−optical behavior of the 20% PEI blend stretched at (T_g + 20 °C) and final stretch ratio 4×.

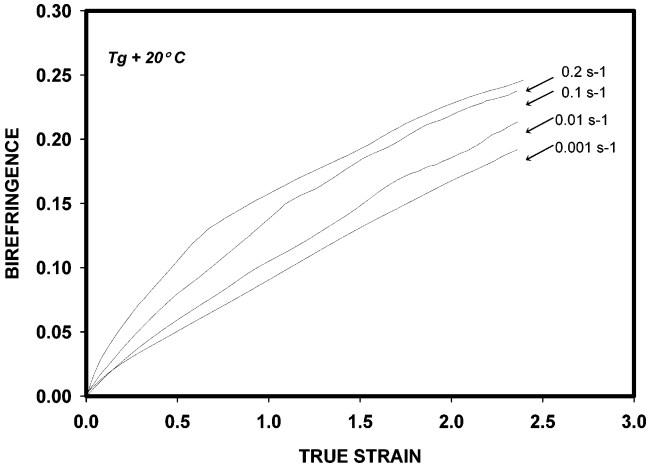

Figure 14. Rate effect on the stress−optical behavior of the 20% PEI blend stretched at (T_g + 20 °C)and final stretch ratio 4×.

Mechanooptical Behavior. The stretching instrument described above is able to provide real-time information on birefringence, true stress, and true strain, allowing us to investigate the stress−optical as well strain−optical behavior simultaneously under a wide range of temperature and strain rate.

Effect of Temperature. To investigate the effect of stretching temperature on the mechanooptical behavior

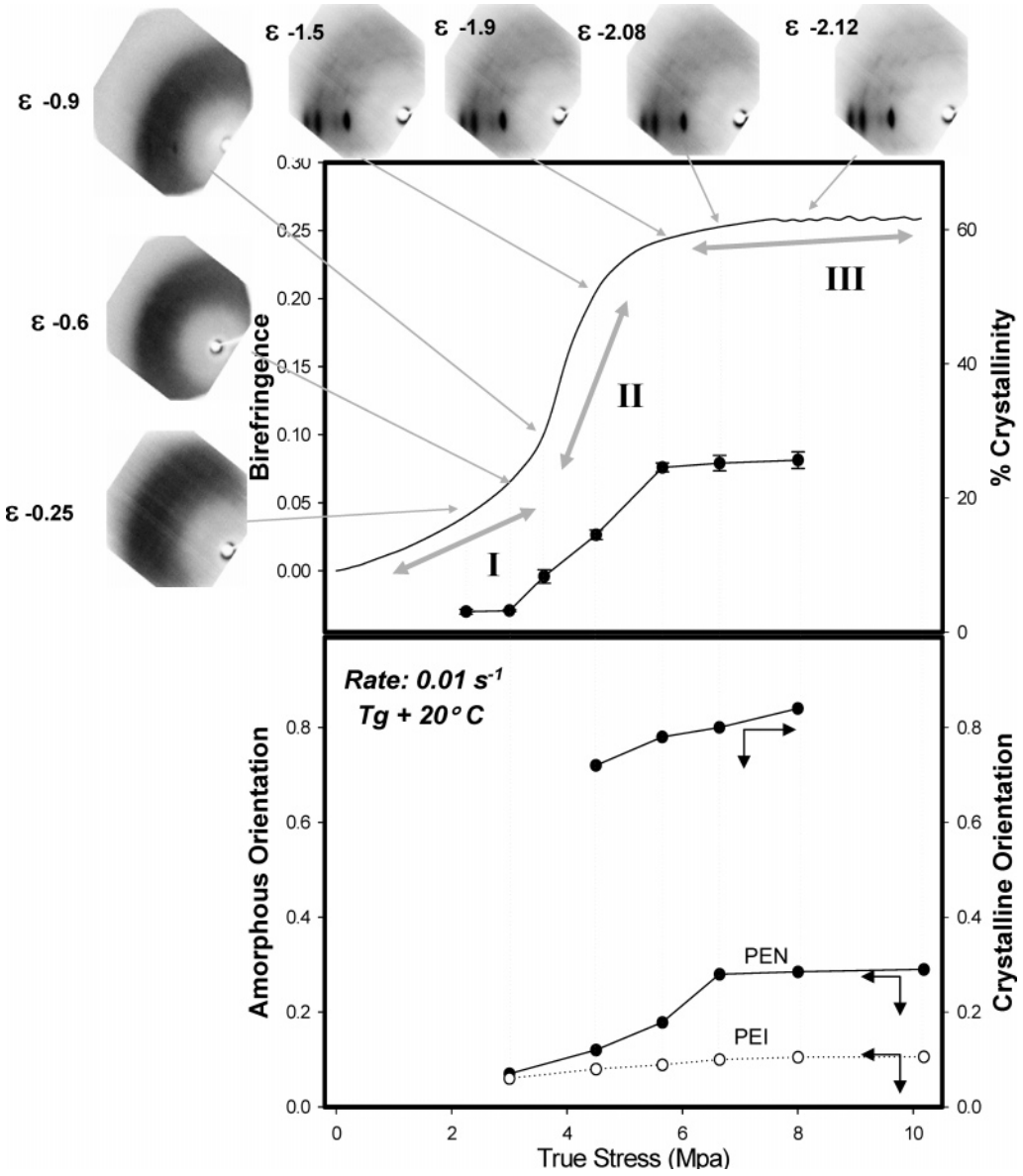

Figure 15. Stress−optical behavior of the 5% PEI blend stretched at engineering strain rate of 0.01 s^{-1} and final stretch ratio 4× with corresponding WAXD patterns, % crystallinity, and orientation analysis (ϵ represents true strain values).

of PEN−PEI blends, the cast films of the blends are stretched above their respective glass transition temperatures, wherein the films exist in a rubbery state while thermal crystallization is still suppressed in this temperature window, as illustrated in Figure 2.

When stretching these blends in the range of T_g +15 °C to T_g + 25 °C, the stress−optical behavior exhibits a glassy behavior as the deformation begins where the stresses increase with little or no change in birefringence (Figures 3 and 4). After exhibiting this glassy component, further stretching of the material shows rubberlike deformation behavior wherein birefringence increases linearly with stress, denoted as "regime I". On further deformation, the deviation from linearity occurs and birefringence increases steeply with stress. Following this "regime II" behavior, birefringence starts to reach a plateau while stresses increase significantly in the final stage "regime III" as the chains reach their finite chain extensibility. Thus, the stress−optical behavior in this temperature range is characterized as regime I−II−III behavior with an initial glassy component.

When the material is stretched at temperatures near the T_g (below T_g + 15 °C), glassy behavior exists in the initial deformation stage which is much more pronounced wherein the stresses corresponding to the glassy component increase with decreasing temperature (Figure 3). As the deformation proceeds, the material comes out of this glassy behavior and exhibits rubberlike deformation following "regime I", the slope of which decreases with increasing temperature. Following this regime I behavior the birefringence starts to reach a plateau with significant stress increase, exhibiting regime III behavior. The regime II wherein birefringence rises steeply with stress is completely absent. So the stress−optical behavior close to T_g is characterized by a regime I−III behavior with an additional glassy component and the absence of the regime II.

When stretching is undertaken at temperatures higher than T_g + 25 °C, the initial glassy component becomes completely absent, and the stress−optical behavior begins with regime I, and further deformation exhibits regime II and III in the stress−optical behavior which is successively eliminated with higher stretching tem-

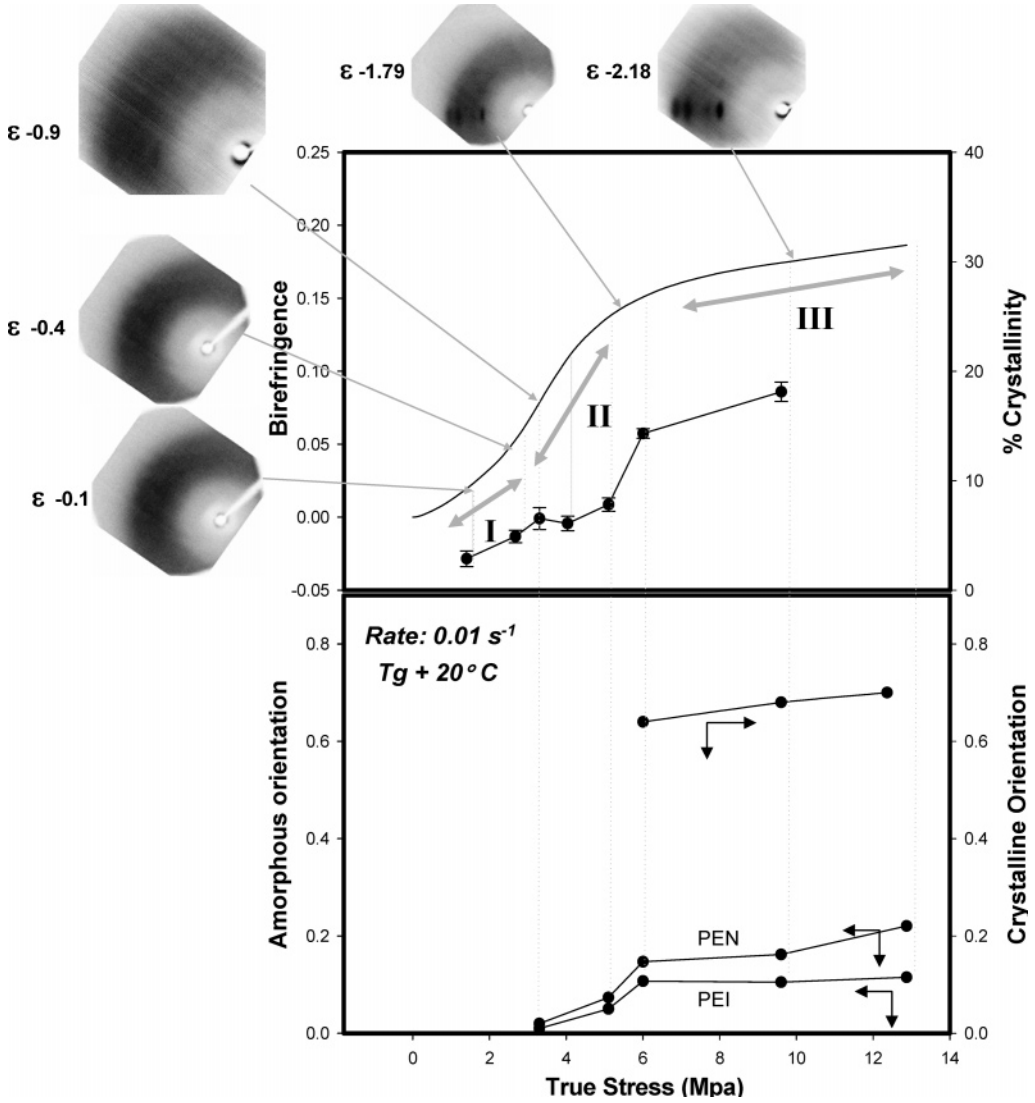

Figure 16. Stress−optical behavior of the 20% PEI blend stretched at engineering strain rate of 0.01 s^{-1} and final stretch ratio 4× with corresponding WAXD patterns, % crystallinity, and orientation analysis (ϵ represent true strain values).

peratures as chain relaxation becomes dominant with increasing temperature (Figures 3 and 4). As illustrated in Figure 3, stretching above 165 °C no longer exhibits the final regime III, and stretching at even higher temperatures around 180 °C the stress−optical behavior consists only of the initial linear regime I.

Plotting the slopes of the glassy component and the regime I for different temperatures above the T_g (Figure 5) shows that, beyond a critical temperature approximately $1.25T_g$ (°C) or $1.08T_g$ (K), the glassy component disappears, and the regime I slope becomes equal to the stress−optical constant and remains constant beyond this critical transition point. This transition is also evident at 150 °C for 5% PEI and at 165 °C for 20% PEI concentration in the strain−optical behavior of the PEN/PEI blends (Figures 6 and 7). Beyond these temperatures the strain−optical behavior changes from near-linear behavior to nonlinear behavior. At the point of transition, there is a significant change in the shape of the curves, which is interpreted as if the material undergoes relaxation to a much higher degree from this point onward. This temperature range of transition is coincidently where Boyer and co-workers have observed a liquid−liquid transition temperature.[21,22] The liquid−Liquid transition (T_{ll}) has been defined as a temperature that separates the two states designated as "fixed liquid" and "true liquid" in a polymer on the basis of their rheological behavior. It is not considered as a thermodynamic transition as it is influenced by the rate of deformation as will be described below. According to this concept, between the T_g and the T_{ll} there are segmental "crystals" that prevent the material from behaving as a true liquid as they act as additional junction points in a physical network made up of entanglements. Increasing the temperature beyond the T_{ll}, these segmental correlations break down, or in other words "segmental melting" occurs. It is clearly observed that when stretching below the T_{ll} in PEN/PEI blends, the prevailing segmental interactions do not allow the material to exhibit rubbery deformation because the energy applied to deform the material at this point is used to break this segmental correlations, leading to high stresses in the system with little increase in birefringence. As soon as these preexisting "segmental crystals" disintegrate beyond the T_{ll}, the material starts showing rubbery deformation with the regime I following the stress−optical rule, and the strain optical behavior after this transition becomes completely nonlinear, indicating no inherent network holding the material anymore which makes it behave as a true liquid.

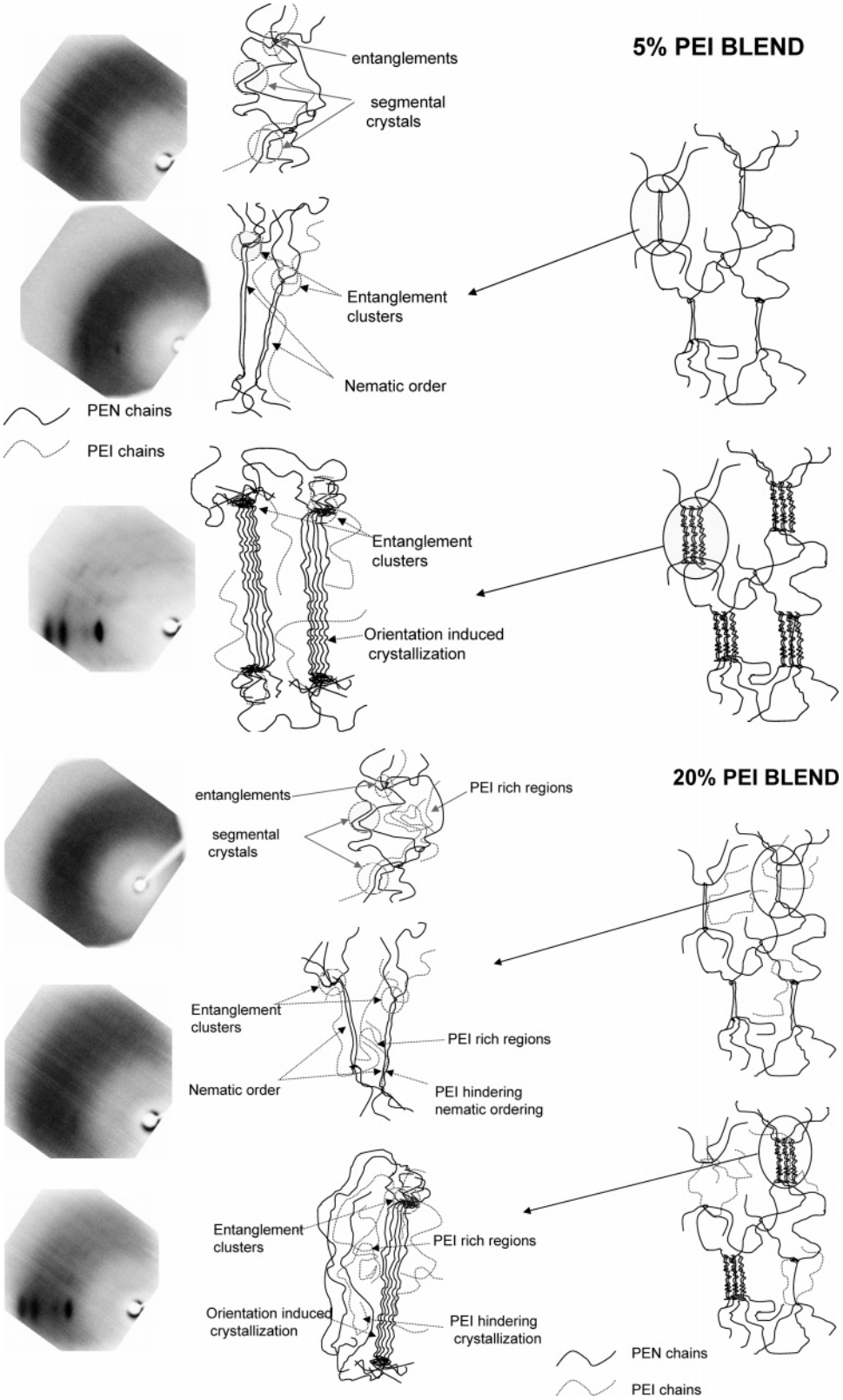

Figure 17. Structural models of (a) 5% and (b) 20% PEI blends.

Relaxation clearly dominates the mechanooptical behavior with increasing the temperature further, as shown in Figures 3 and 4. As we increase the stretching temperature above 155 °C for 5% PEI and 165 °C for 20% PEI, the material undergoes significant relaxation necessary for the chains to crystallize but does not allow the chains to reach their finite chain extensibility; hence, the stress−optical behavior shows regime I and II, but regime III corresponding to finite chain extensibility is absent though all these samples were stretched to the same macroscopic (engineering) stretch ratio of 4×. With further increasing the temperature to 165 °C for 5% PEI and 180 °C for 20% PEI, the material exhibits only the regime I of the stress−optical behavior. This is because chain relaxation is so dominant at this temperature that the chains are not able to reach the

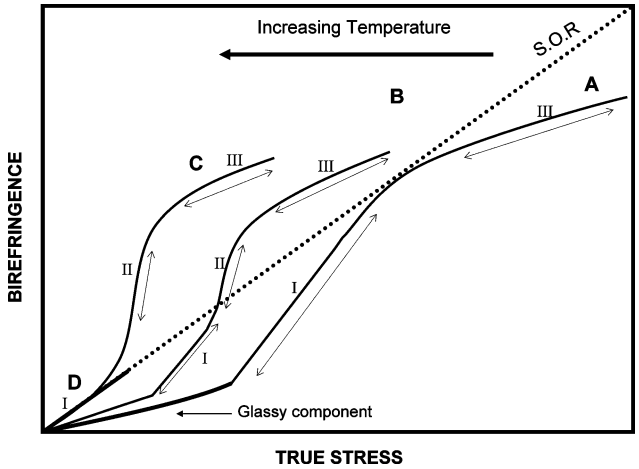

Figure 18. Generalized stress−optical behavior for slow-crystallizing polymers as a function of temperature.

critical orientation required for them to crystallize and also to reach their finite chain extensibility.

Effect of Blend Composition. The effect of blending amorphous PEI in PEN was investigated on the mechanical as well as the optical properties of PEN. True stress−true strain behavior of the PEN−PEI blends as a function of blend composition is shown in Figure 8. Because of the variations in T_g with composition, the processing temperature was chosen at T_g + 20 °C to place these materials under "roughly" equivalent thermal conditions during deformation. These true mechanical data are the true representation of the material response to the deformation as the measurement system continuously measures the instantaneous cross-sectional area. The off-line vs on-line thickness measurements are shown in Figure 1. It is also important to emphasize that all the measurements (birefringence, stress, and strain) are referring to the mid-symmetry plane of the samples.

One of the important characteristic of a material observed in Figure 8 is the onset of strain hardening that influences the thickness uniformity of the material during processing and hence the final properties of the product. Initial addition of PEI (5%) into PEN slightly delays the onset of strain hardening as observed in the figure. Addition of 5% PEI in PEN results in a completely miscible system (ΔT_g is less than 10 °C). Because of this intimate level of mixing, the conformation and packing of PEN molecules in the blend may not be able to achieve the state in the pure PEN as they have to accommodate the rigid and bulky PEI molecules leading to slight retardation of the onset of strain hardening. At this low concentration the stiff PEI molecules are well dispersed in PEN, and hence they suppress the formation of a physical network formed mostly of PEN crystallites as the PEI chains act as disruptors. However, further addition of PEI chains causes a decrease in the onset of strain hardening as the mobility of the PEN chains is hindered due to the "rigidification effect" caused not only by the introduction of stiff PEI molecules but also due to the PEI-rich microheterogeneities that start to form in the blend (ΔT_g increases beyond 10 °C). These localized PEI-rich microheterogeneities act as barriers to the free movement of PEN chains by acting as additional physical network nodes, leading to an early onset of strain hardening.

With the addition of PEI, the final true strain achieved in the blend increases. This is attributed to the decrease of crystallizability with the addition of PEI in which the rapid formation of long range connected tight network is suppressed, allowing larger deformations to take place in the mid-plane of the sample where all the measurements are made.

Optical Behavior. The birefringence change during deformation follows different stages, depending on the blend composition as shown in Figure 9. For PEN, 5% PEI, and 10% PEI blend compositions the birefringence initially increases nonlinearly with true strain followed by a dip in the slope which becomes less pronounced with addition of PEI. Then a sharp rise of birefringence is observed, and finally the birefringence increases linearly with true strain. For 20% PEI blend composition the birefringence initially increases nonlinearly with true strain, and on further deformation birefringence essentially follows a linear increase with true strain until the end of the deformation process. The dip in the slope occurring in the prior case completely evens out with the addition of 20% PEI in the blend. Final birefringence levels reached in the material are greatly dependent on the blend composition, decreasing with increasing PEI concentration.

Strain Rate Behavior. The true (local) strain rate extracted from the temporal variation of true strain behavior for different blend compositions is shown in Figure 10 for 0.01 s^{-1} (macro)stretching rate. The results indicate that at constant crosshead separation speed the strain rate at the midsection of the sample is not constant. At early stages of deformation, the strain rate is around 0.01 s^{-1} for all the blends, following affine deformation behavior as it corresponds to the stretching rate applied by the stretching machine. Then the strain rate sharply rises in the case of PEN, 5% PEI, and 10% PEI blends, signifying spontaneous deformation at the midsection of the sample where the measurement is made. The sharpness significantly decreases with further addition of PEI, and finally with the addition of 20% PEI the peak significantly broadens, showing up only as a hump completely eliminating the sharpness in the peak. Finally, the strain rate rapidly decreases, ultimately reaching almost zero values at the midsection of the sample except for 20% PEI blend, which shows nonzero strain rates even at the end of the deformation process.

The strain rate changes as a function of true strain are directly correlated to the birefringence changes observed in the material. In the affine deformation stage, birefringence increases monotonically with true strain for all the blends. When the strain rate accelerates sharply in the case of PEN, 5% PEI, and 10% PEI blends, birefringence as also accelerates sharply as shown by short vertical line marks indicating the rise in true strain rate as well as birefringence. With further stretching, the strain rate reaches a maximum value which also marks the end of the steep birefringence increase (open circular marks in Figures 9 and 10). Beyond this point, the strain rate starts decreasing (Figure 10) while the birefringence linearly increases with true strain (Figure 9). In the 20% PEI blend, the second stage of sharp acceleration in the strain rate, as well as birefringence, is suppressed, and the strain rate increase exhibits a mild plateau and then decreases on further deformation. A possible explanation for these results is that after a certain level of chain elongation a process of spontaneous orientation primarily induced by the "coil to stretch"[23,24] transition as well as necking

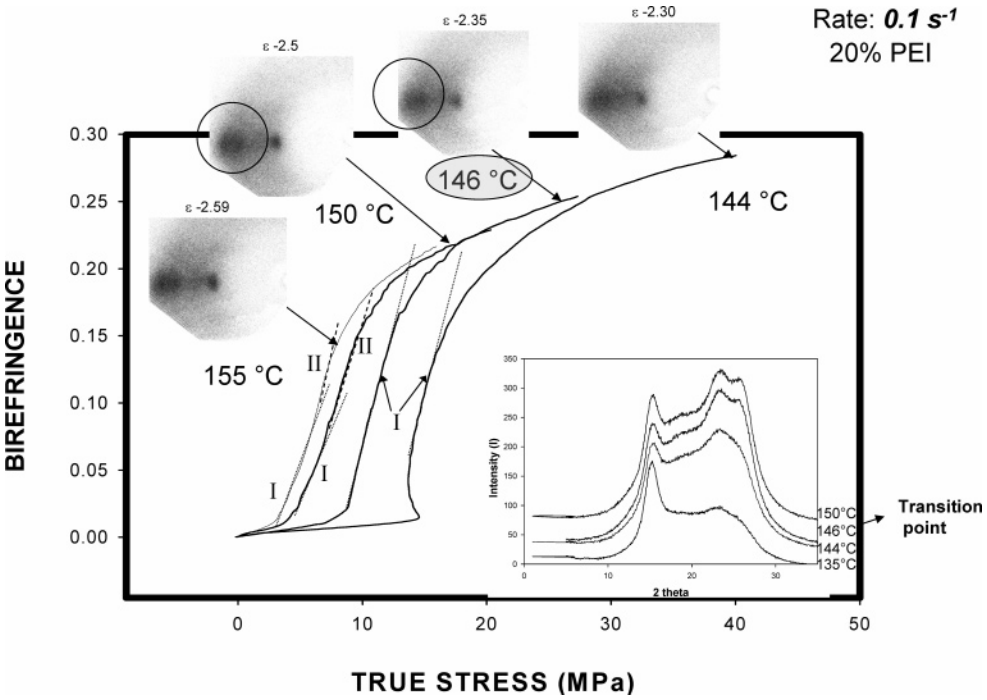

Figure 19. Stress−optical behavior of the 20% PEI blend stretched at engineering strain rate of 0.1 s^{-1} and final stretch ratio 4× with corresponding WAXD patterns indicating nematic-to-crystalline transition.

occurs in 100% PEN as well as 5% PEI and 10% PEI blends, leading to a sharp rise in birefringence and strain rate. Addition of 20% PEI eliminates necking and hence suppresses the resulting spontaneous deformation process, leading to a uniform stretching behavior as shown in the figure.

Mechanooptical Behavior. The influence of PEI composition on the stress−optical behavior of PEN is shown in Figure 11, wherein all the blends are stretched at the processing temperature 20 °C higher than their T_g (T_g + 20 °C) and rate (0.001 s^{-1}). 0% PEI and 5% PEI compositions stretched under these conditions show three distinct stress−optical regimes (shown by arrrows) similar to the behavior described in an earlier paper for pure PEN[25] and PLA.[26] In 10% PEI and 20% PEI blend films, an additional glassy component with a much lower slope appears (shown with stars). Stretching beyond this glassy regime, the material follows the traditional three-regime behavior. PEN shows similar glassy behavior when it is stretched very close to T_g, specifically at and below (T_g + 10 °C).[26] This shows that the addition of PEI in the blend makes the glassy component appear even at higher temperatures, due primarily to the broadening of the glass transition range (Figure 2a).

The stress−optical coefficient (SOC) of the blends determined from the stress−birefringence curves obtained at temperatures beyond the T_{ll} (Figures 3 and 4) is plotted as a function of blend composition in Figure 12. The films with 5% PEI exhibit a SOC of 20 GPa^{-1}, which decreases to 17.3 GPa^{-1} for 20% PEI concentration. These results indicate that the intrinsic birefringence of PEI is lower than PEN. We, however, could not find published intrinsic birefringence for PEI. The stress−optical constant for pure PEN was determined by Martins et al.,[25] Ito et al.,[7] Izuka et al.,[27] Inoue et al.,[28] and Okamoto et al.[17] and reported the following values: 27.5, 13, 16.1, 12.4, and 18 GPa^{-1}, respectively. These results are in the same range of the results obtained in this investigation.

The regime II slope in the stress−optical behavior is characterized by fast increase in birefringence for PEN and 5% PEI blends and is also suppressed with further addition of PEI (Figure 11). The total birefringence developed in the blends also decreases with the addition of PEI while the stresses developed increase as seen in Figure 11.

Effect of Stretching Rate. The effect of the deformation rate on the stress−optical and strain−optical behavior of PEN−PEI blends is shown in Figures 13 and 14. In stress−optical behavior, the increase in the rate of stretching intensifies the additional glassy component. This is very similar to the effect observed with decreasing the stretching temperature. Stretching the polymer at high enough rates or low enough temperatures suppresses chain mobility, leading to high stresses to break the segmental interactions causing this glassy behavior. We suspect that these segmental "crystals" associated with the glassy behavior form a long-range network that substantially breaks up at the yield point (see 0.2 s^{-1} curve), and the ensuing flow—and consequent birefringence increase—requires less energy input into the material, leading to rapid rise of birefringence.

Strain−optical behavior is quite linear beyond a brief initial nonlinear transition region at low strains and low to moderate strain rate while it becomes increasingly nonlinear with the increase in strain rate at and beyond 0.1 s^{-1}.

Structural Studies. To assess the structural mechanisms responsible for the regimes observed in real-time mechanooptical behavior, we have performed off-line characterization on samples rapidly frozen after being stretched to a series of deformation levels. In this process we do have some relaxation that could influence the final structure. Nevertheless, the trends in the structural organization processes can be extracted through such an experimental exercise. The results of off-line X-ray, DSC crystallinity, and IR dichroism analysis together with the stress−optical behavior of films stretched at T_g + 20 °C are presented in Figures

15 and 16. The material stretched under these conditions is still below the T_{ll} transition. As indicated earlier, the films containing 5% and 20% PEI exhibit three different stress−optical regimes along with an additional glassy behavior. Until the regime I, X-ray patterns and DSC crystallinity measurements show that material remains in the amorphous state with crystallinity levels remaining well below 10%. The material at this point is composed of amorphous polymer chains with prevalent "segmental crystals" as well as entanglements existing throughout the material, as depicted in the structural model (Figure 17). Deviation into the regime II of the stress−optical behavior accompanies the development of very sharp equatorial (010) peak, indicating the presence of very highly oriented chains with substantial translational disorder as evident by the concurrent absence of off-equatorial peaks. This is a clear signature WAXS pattern for a "nematic-like" order. We envision these regions are junctions of the long-range network that, once formed, cause a rapid increase of birefringence (Figure 17). This resulting nematic-like order acts as a precursor to the crystallization process. Considering the change in true strain rate with true strain (Figure 10), it is observed that the steep rise in strain rate occurs a little before the nematic order and crystallinity starts to appear. This indicates that after a certain level of deformation a long-range "connected" network of chains is formed as the "coil-to-stretch" transition occurs facilitating efficient transmission of the stretching forces throughout the material, causing the steep rise in strain rate as well as birefringence. Further stretching leads to the appearance of higher order peaks in the X-ray pattern, and the off-equatorial peaks start to emerge, suggesting development of a regular three-dimensionally ordered crystal structure in the material that becomes more distinct as we proceed into regime III (Figure 17). The development of crystallinity follows a steep slope in the regime II but reaches a plateau going into regime III, indicating no significant structural changes happening from this point onward.

Effect of Blend Composition. Addition of PEI into PEN makes the X-ray patterns more diffuse, and the appearance of off-equatorial peaks in the X-ray patterns for 20% PEI blend is observed only in regime III while in the 5% PEI blend they appear in regime II of the stress−optical behavior, indicating suppressed relaxation with PEI addition. Appearance of a sharp (010) peak in the case of 5% PEI blend has a much higher azimuthal spread in 20% PEI blend, indicating suppressed orientation with PEI addition (Figure 17a). The degree of crystallinity developed in 20% PEI is about 18%, which is lower by about 40% when compared to 5% PEI sample, confirming that PEI suppresses crystallization of PEN due to the dilution effect.

The orientation factor for amorphous regions of PEN chains is relatively low in the beginning and through the initial crystallization process. After a sufficient degree of crystallinity in the material, the orientation of amorphous PEN chains picks up and increases until the beginning of regime III, indicating that after the crystalline network is formed, further stretching pulls the amorphous chains more forcefully as the stresses are felt more evenly throughout the whole sample. Further stretching into regime III does not cause any significant orientation of PEN chains in the case of the 5% PEI blend. In the 20% PEI blend the PEN chains

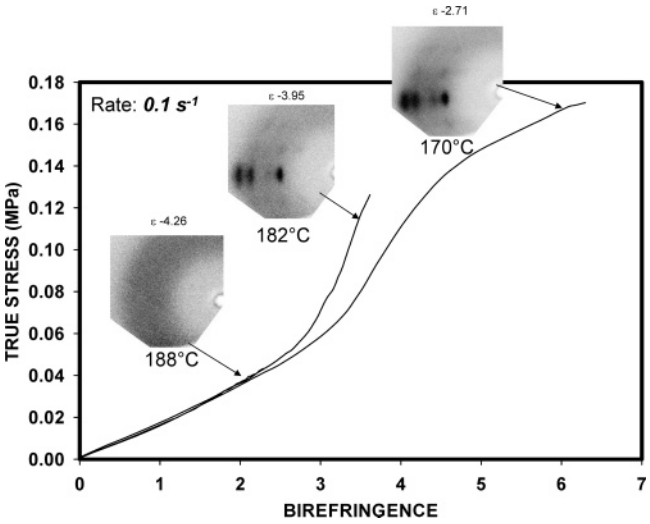

Figure 20. Stress−optical behavior of the 20% PEI blend stretched at engineering strain rate of 0.1 s^{-1} and final stretch ratio 4× with corresponding WAXD patterns indicating crystalline-to-amorphous transition.

still continue to orient but at a much lower rate as the crystallinity levels are suppressed, not locking the material and allowing it to slowly deform. Orientation of the PEI chains, however, remains distinctively low throughout the stretching cycle in all the blends and barely reaches an orientation factor of 0.1. The decrease in birefringence with increasing PEI content as discussed earlier is partly due to the lower PEI intrinsic birefringence, the decrease in degree of crystallinity, and the lower crystalline as well as amorphous orientation as determined by WAXS and IR dichroism techniques.

Identification of Phases. *Nematic−Crystalline Transition.* As shown in Figure 19 for 20% PEI, the stress−optical behavior has a significant initial glassy behavior at 144 °C, and at the end of stretching to a true strain of 2.3, the WAXD pattern exhibits nematic behavior as the (010) is the only distinct diffraction spot observed on the equator. Where we expect the ($\bar{1}$10) and (100) peaks, we observe only a very broad and indistinct amorphous peak. When the temperature is raised to 146 and 150 °C, we begin to see the first evidence of distinct ($\bar{1}$10) and (100) peaks as evidenced in the equatorial profiles presented in the inset. Concurrently, we also observe a change in the slope of regime I beyond the glassy behavior, and a positive deviation into regime II is observed in the stress−optical behavior as schematically described in Figure 18 (A changes to B). We take this positive deviation into regime II as the first evidence of strain-induced crystallization.

Crystalline−Amorphous Transition at High Temperature. As shown earlier, when we progressively increase the processing temperature from 170, 182, and 188 °C, regimes III and II disappear, leaving only regime I (Figure 20). The corresponding WAXD patterns indicate that even though much higher true strain levels are attained at 188 °C, the strain-induced crystallization is eliminated, and the material remains amorphous while remaining in regime I as schematically described in Figure 18 (C changes to D). This range between 182 and 188 °C defines a semicrystalline−amorphous dynamic phase boundary.

T_{ll} Transition. As we discussed earlier, when the slopes of the photoelastic constant becomes equal to the regime I slope, we define a temperature as the T_{ll} for

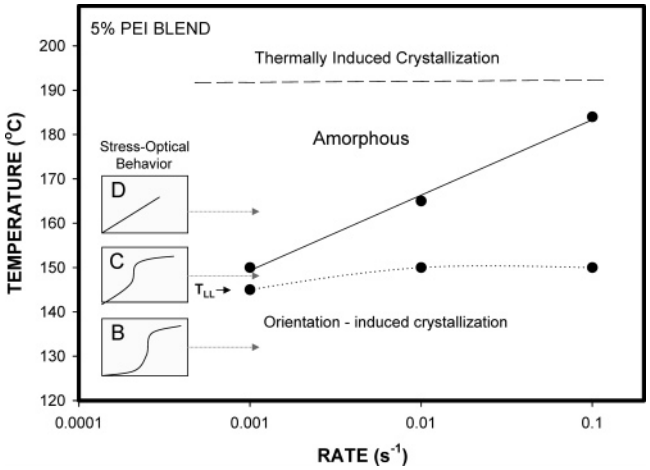

Figure 21. Dynamic phase diagram for the 5% PEI blend as a function of temperature and engineering strain rate.

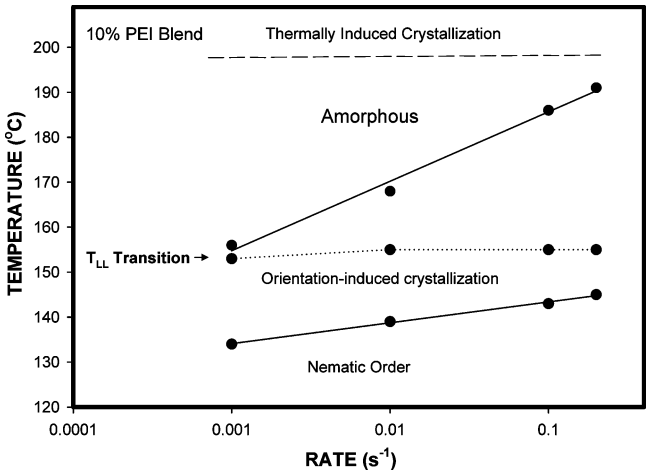

Figure 22. Dynamic phase diagram for the 10% PEI blend as a function of temperature and engineering strain rate.

that specific composition and rate. This T_{ll} occurs at approximately $1.25T_g$ (°C) or $1.08T_g$ (K). The transition from B to C shown schematically in Figure 18 describes the change in the stress−optical behavior.

Dynamical Phase Diagrams. On the basis of the criteria established above, we determined the dynamical phase diagrams for PEN/PEI compositions containing 5, 10, and 20% PEI stretched at different rates. These are shown in Figures 21−23. Three critical structural transitions were observed: (1) nematic−crystalline transition; (2) crystalline−amorphous transition; (3) liquid−liquid (T_{ll}) transition. In the present definition of the "dynamical phase diagram", we certainly do not imply that the rules governing classical thermodynamic phase diagram such as reversibility of phases and time independence are obeyed. It merely reflects the dependency of phases on the rate and temperature of deformation used in stretching. In the films containing 5% PEI we do not observe nematic order at low temperatures. This phase appears at 10% and becomes quite clear at 20% PEI concentration. We attribute the appearance of nematic order to suppression of the orientation relaxation in the presence of stiff PEI chains in PEN. The phase boundary is linear in this logarithmic scale. The T_{ll} transition is rate dependent at low rates, but it becomes insensitive at rates beyond about 0.001 s^{-1}. The phase boundary between orientation-induced crystallization and amorphous phase has stronger rate dependence while the relationships remain linear in the logarithmic scale.

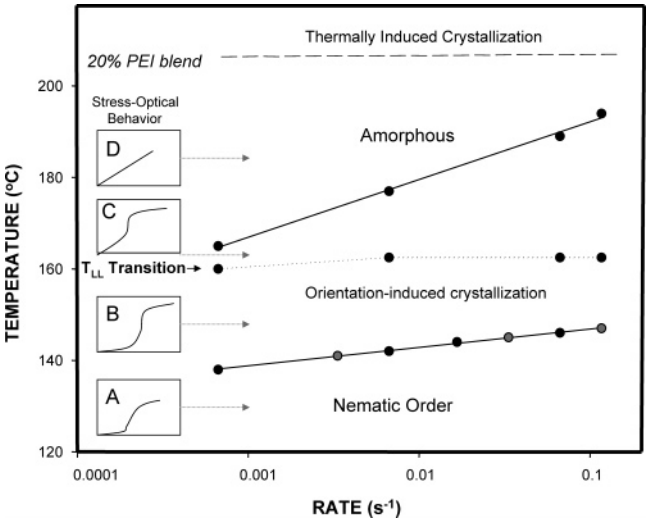

Figure 23. Dynamic phase diagram for the 20% PEI blend as a function of temperature and engineering strain rate.

IV. Conclusions

PEN/PEI blends exhibit a three-regime nonlinear stress−optical behavior. The liquid−Liquid transition below which the stress optical behavior includes an initial glassy component was attributed to "stiff" segmental correlations that disappear above the T_{ll}. At low stretching temperatures, the films remain in a nematic-like state that converts into orientation-induced crystallization at intermediate temperatures. At high enough temperatures, we found an additional temperature window in which stretching yields a completely amorphous structure due to significant orientation relaxations coupled with the absence of thermally activated crystallization. On the basis of these quantitative results, "dynamical phase diagrams" were constructed.

References and Notes

(1) Toki, S.; Valladares, D.; Sen, T. Z.; Cakmak, M. *ANTEC Proc.* **2001**, 1830.
(2) Koike, Y.; Cakmak, M. *Polymer* **2003**, *44*, 4249.
(3) Lee, S. W.; Cakmak, M. *Polymer* **1995**, *36*, 4039−4054.
(4) Kim, J. C.; Cakmak, M. *J Appl. Polym. Sci.* **1997**, *65*, 2059.
(5) Murakami, S.; Yamakawa, M.; Tsuji, M.; Kohjiya, S. *Polymer* **1996**, *37*, 3945−3951.
(6) Schoukens, G.; Verschuere, M. *Polymer* **1999**, *40*, 3753−3761.
(7) Ito, H.; Suzuki, K.; Kikutani, T.; Nakayama, K. PPS 18 conference proceedings, Portugal, 2002.
(8) Blanton, T. N. *Powder Diffr.* **2002**, *17*, 125−131.
(9) Miyata, K.; Kikutani, T.; Norimasa, O. *J. Appl. Polym. Sci.* **1997**, *65*, 1415−1427.
(10) Wu, G.; Li, Q.; Cuculo, J. A. *Polymer* **2000**, *41*, 8139−8150.
(11) Mahendrasingam, A.; Blundell, D. J.; Martin, C.; Fuller, W.; Mackerron, D. H.; Harvie, J. L.; Oldman, R. J.; Riekel, C. *Polymer* **2000**, *41*, 7803−7814.
(12) Koike, Y.; Cakmak, M. *Macromolecules* **2004**, *37*, 2171−2181.
(13) Valladares, D.; Toki, S.; Sen, T. Z.; Yalcin, B.; Cakmak, M. *Macromol. Symp.* **2002**, *185*, 149−166.
(14) Ryu, D. S.; Inoue, T.; Osaki, K. *Polymer* **1998**, *39*, 2515−2520.
(15) Okamoto, M.; Kubo, H.; Kotaka, T. *Macromolecules* **1998**, *31*, 4223−4231.
(16) Kroger, M.; Luap, C.; Muller, R. *Macromolecules* **1997**, *30*, 526−539.
(17) Ouchi, I. H.; Aoki, S.; Shinotsuma, T.; Asai, M.; Hosoi, *Proc. 17th Jpn. Congr. Mater. Res*., March 1974; p 217.
(18) Mencik, Z. *Chem Prum.* **1967**, *17*, 78.

(19) Cheng, S. Z. D.; Wunderlich, W. *Macromolecules* **1988**, *21*, 789−797.
(20) Premnath, V. *Macromolecules* **1995**, *28*, 5139−5143.
(21) Boyer, R. B. *Polym. Yearbook* **1998**, 234−337.
(22) Stadnicki, S. J.; Gillham, J. K. *J. Polym. Sci.* **1976**, *20*, 1245−1276.
(23) Odell, J.; Keller, A.; Miles, M. J. *Polymer* **1985**, *26*, 1219−1226.
(24) Hunkeler, D.; Nguyen, T. Q.; Kausch, H. H. *Polymer* **1996**, *37*, 4257−4269.
(25) Martins, C. I.; Cakmak, M. *Macromolecules* **2005**, *38*, 4260−4273.
(26) Mulligan, J.; Cakmak, M. *Macromolecules* **2005**, *38*, 2333−2344.
(27) Iizuka, N.; Yabuki, K. *Sen-I Gakkaishi* **1995**, *51*, 463−469.
(28) Inoue, T.; Matsui, H.; Murakami, S.; Kohjiya, S.; Osaki, K. *Polymer* **1997**, *38*, 1215−1220.

MA0511595